

Review of Analysis and Modeling Techniques for Incompressible, Turbulent Bluff-Body Wakes

Logan D. Halstrom* and Federico Zabaleta†
University of California, Davis, California, 95616

abstract here LH&FZ

Nomenclature

LH&FZ

ρ = density, kg/m^3

Subscripts

(∞) = freestream quantity

Acronyms

CFD = Computational Fluid Dynamics

I. Introduction

BODIES When a body moves in a fluid, it experiences different forces, such as lift and drag. Drag can occur due to a difference in velocity in the surface of the body and the mean flow, in which case we call it friction drag. This friction is associated with the development of boundary layers and it scales with the Reynolds number. If the drag is due to a difference in pressure through the surface of the body, then we call it pressure drag or viscous induced drag. This drag is usually associated with separation of the flow and the formation of a wake downstream the body. In real flows, drag is composed by the combination of both. The effect of frictional drag is usually more relevant for attached flows while the pressure drag prevails in separated flows.

We can analyze the effect of friction and pressure drag by analyzing the flow around a flat plate. If the flat plate is oriented in the direction of the flow, then the friction drag will be important while the pressure drag will be almost negligible. On the other side, if the flat plate is oriented perpendicular to the flow, then the difference of pressure between both sides of the plate will be much more important than the effect of the friction, and so the pressure drag will be dominant.

When the drag of a body is dominated by viscous drag, we define the body as a streamlined body. Flat plates (oriented in the direction of the flow) or airfoils with a small angle of attack are examples of those. When the flow is

*Graduate Student, Mechanical And Aerospace Engineering Department, One Shields Avenue

†Graduate Student, Civil and Environmental Engineering Department, One Shields Avenue

dominated by pressure drag, we define the body as a bluff or blunt body. Examples of these are squares, cylinders, spheres or airfoil at large angle of attack. Whether a body is considered bluff or streamlined is only a function of its shape and its orientation with respect to the flow.

INSERT FIGURE

II. Flow around a bluff body and transition

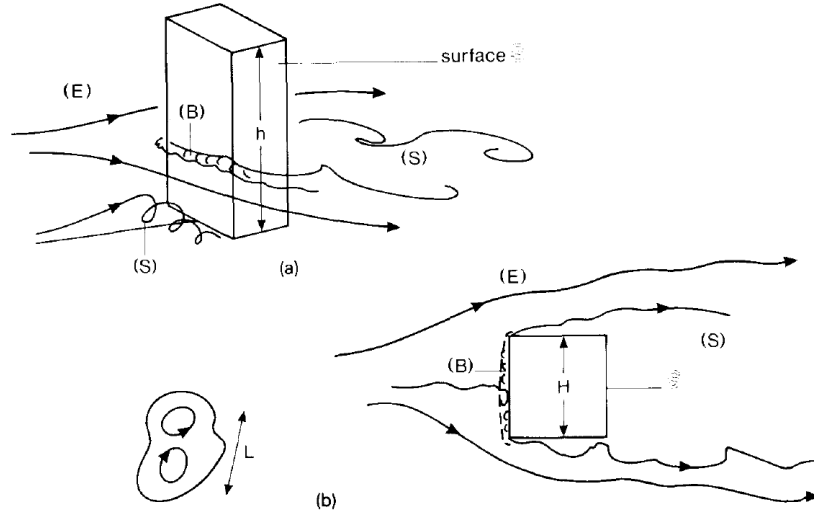


Fig. 1 Regions of disturbed flow. Extracted from [1]

A. Steady laminar wake

B. Periodic Laminar Regime

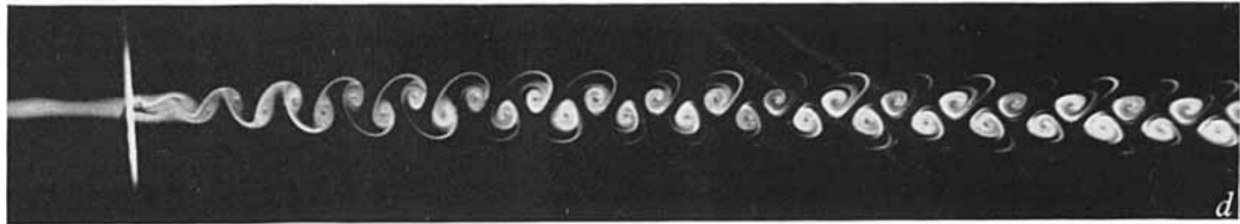


Fig. 2 Kármán-Bénard eddy street at $Re = 100$. Extracted from [2]

C. Transition in wake state



Fig. 3 Transition in wake at $Re = 190$. Extracted from [2]



Fig. 4 Transition in wake at $Re = 344$. Extracted from [3]

D. Transition in shear layers state

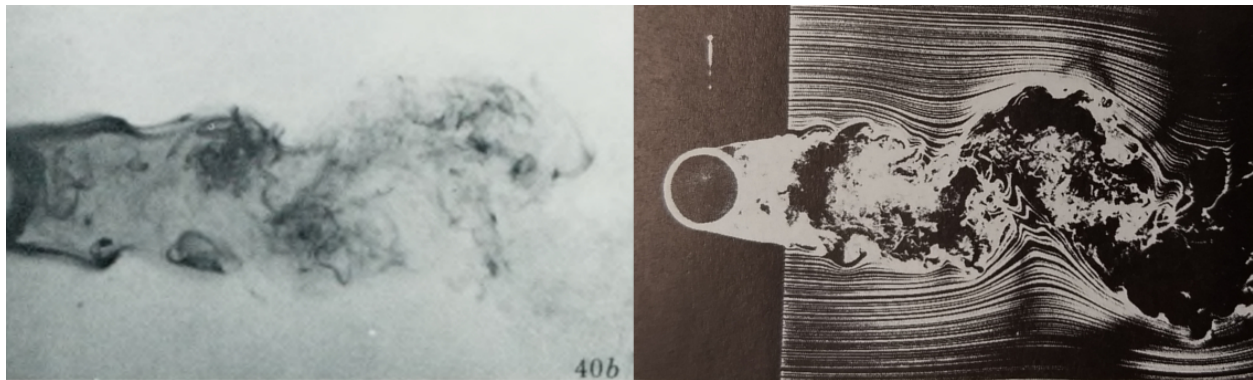


Fig. 5 Transition in free shear layer. Left: $Re = 1083$. Extracted from [3]. Right: $Re = 8000$. Extracted from [4]

E. Transition in boundary layer

F. Fully turbulent state

III. Free stream turbulence and non-uniform free stream

- Driving Physical Phenomena *FZ*

- differences from potential flow
- blunt/bluff body definition, differences from streamlined body flow
- massively separated flow
- base pressure
- wake

- Real World Applications *LH*

- parachute
- reentry capsule
- vehicles
- buildings
- show similarity between cylinder/sphere wake and more complex bluff body
- relevance: stability, acoustics, buffeting/unsteady loads, mixing

Big whorls have little whorls, which feed on their velocity, and little whorls have lesser whorls, and so on to viscosity (in the molecular sense). Richardson (1922) [5]

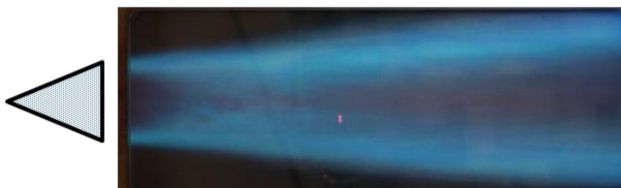


Fig. 6 Bluff-body flame holder [6]

Bluff body stabilized flame is widely used in various industrial systems in which the flow speed is much higher than the flame speed. Without a continuous ignition source the flame would be blown out. Hence the gutter/bluff body is usually placed with its axis perpendicular to the flow direction. The gutter traps the hot gas downstream of the recirculation zone. The trapped hot gas acts as a continuous ignition source to hold and stabilize the flame. The gutter is usually called as a flame holder or a flame stabilizer [7].

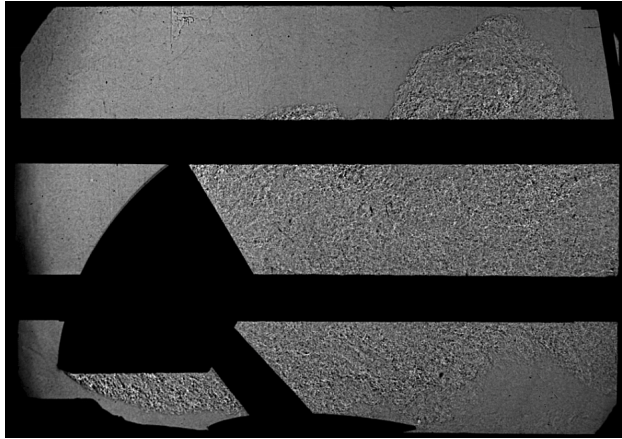


Fig. 7 Shadowgraph wake of orion capsule model M=0.3 [8]

Single frame of high-speed shadowgraph video; M 0.3, AoA = 29.25 deg, ReD = 5.3x106.

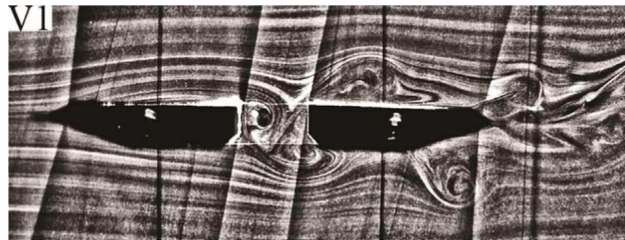


Fig. 8 PIV flow field of bride model similar to tacoma narrows bridge Re=587 [9]

Fig. 11. Instantaneous flow fields around the dynamic model. The corresponding inflow velocities are 0.66 m/s, 0.95 m/s, 1.14 m/s and 1.80 m/s for V1, T1, V2 and T2.

Wake-induced vibration commences in V1 when the shear layer rolls up and the Karman vortex street forms in the central gap



Fig. 9 Streamlines and separated flow over a car in a wind tunnel (NASA/Eric James)

IV. Experimental Methods And Results

FZ

- Historical Study
- Experimental techniques
 - ballistic range?
- Applications
 - Simple cases: cylinder/sphere
 - * Drag vs Re?
 - * Wake velocity profiles?
 - * Wake structure?
 - Sharp vs bluff: sphere vs cube
 - Complex cases: capsule/building

V. Computational Methods and Results

LH

- Historical Study
- Computational techniques
- Applications
 - Simple cases: cylinder/sphere
 - Sharp vs bluff: sphere vs cube
 - Complex cases: capsule/building

A. Turbulence Modeling Aspects

LH

- Brief turbulence model description
 - RANS vs URANS
 - DNS
 - LES (uses DNS) and DES (=Hybrid RANS/LES)
- Compare turbulence model performance for sphere/cylinder
 - DES > URANS > RANS
 - DES = functional LES
 - SAS vs DES?
 - DNS: limited Re
- Shortcomings of each model (and how to address them)
 - URANS
 - DES: only good at sharp separation
 - * “An order of accuracy has not even been proposed for a simulation using both modes within DES”
 - Spalart about hybrid method
 - * grid induced separation (maybe not an issue for bluff bodies)
 - * DES can default to RANS if grid adaptation misses a shear layer
 - * more computational cost than RANS
- Advanced geometries
 - f-15
 - car
 - building
 - capsule
 - chute, landing gear, helicopter, wind turbine

LIST ALL FIGURES HERE, REORDER AND DESCRIBE LATER

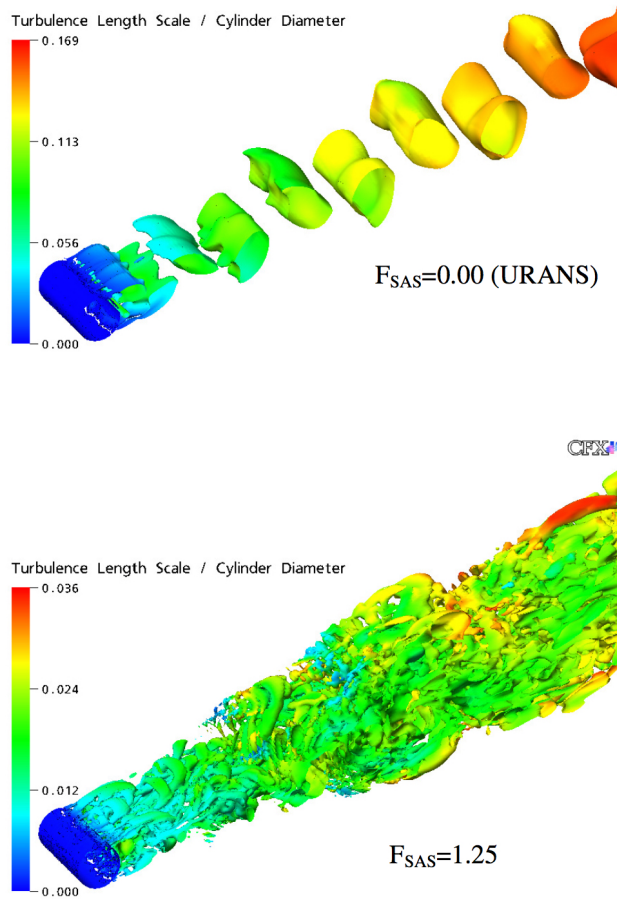


Fig. 10 SAS vs URANS cylinder [10]

Figure 5: Resolved structures for cylinder in crossflow using different constants FSAS Re=3.6e6

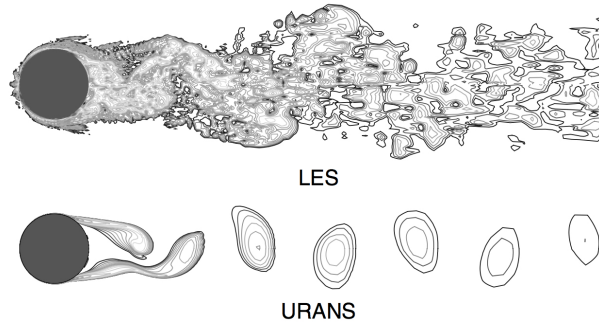


Fig. 11 cylinder les vs urans instantaneous [11]

Instantaneous vorticity magnitude at a given spanwise cut for flow over a circular cylinder at $ReD = 1/4 \cdot 106.25$ contour levels from $xD = U_1/4 \cdot 1$ to $xD = U_1/4 \cdot 575$ (exponential distribution) are plotted.

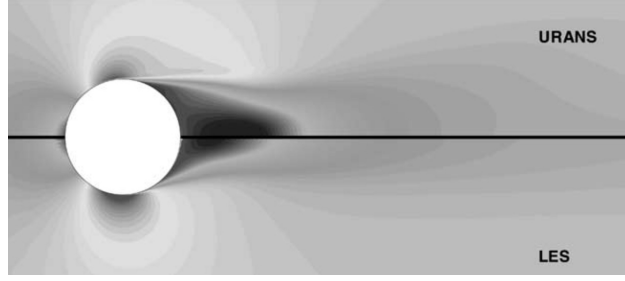


Fig. 12 cylinder les vs urans averaged [11]

Fig. 5. Mean streamwise velocity distribution predicted by LES and URANS. 45 contour levels from $U=U_1 1/4 0:2$ to $U=U_1 1/4 1:7$ are plotted.

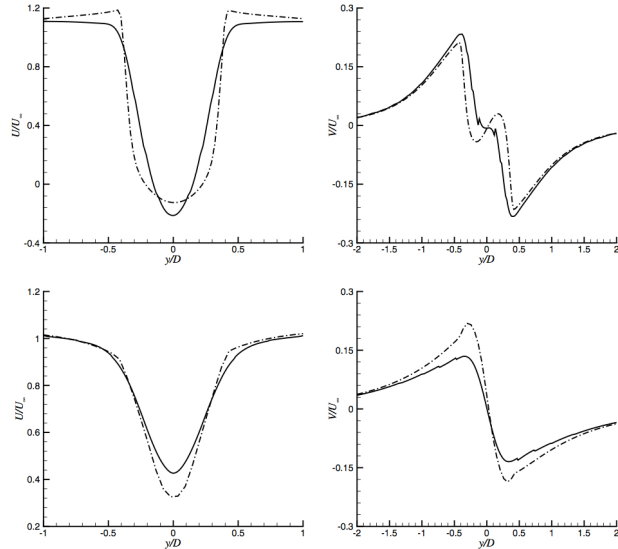


Fig. 13 cylinder les vs urans velocity profiles [11]

Fig. 6. Mean streamwise and vertical velocities at $x=D 1/4 0:75$ (upper figures) and $x=D 1/4 1:50$ (lower figures):
 (—) LES; (--) URANS

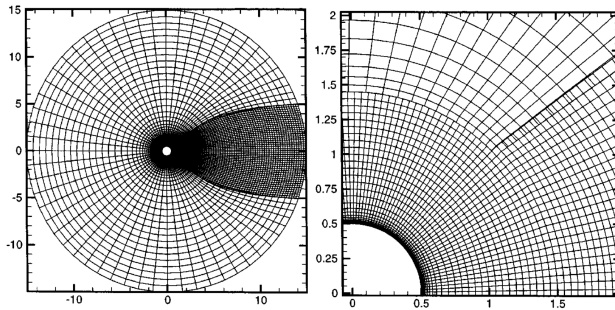


Fig. 14 cylinder les vs rans grid [12]

Figure1. Medium computational grid, CaseTS2. Innerblock 150×36 , wakeblock 74×36 , outer block 59×30 . The three blocks meet near $x = 1.06$, $y = 1.03$. Grid for spalart cylinders.

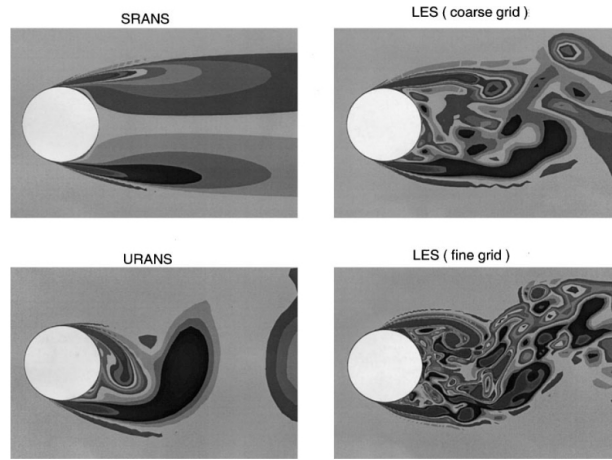
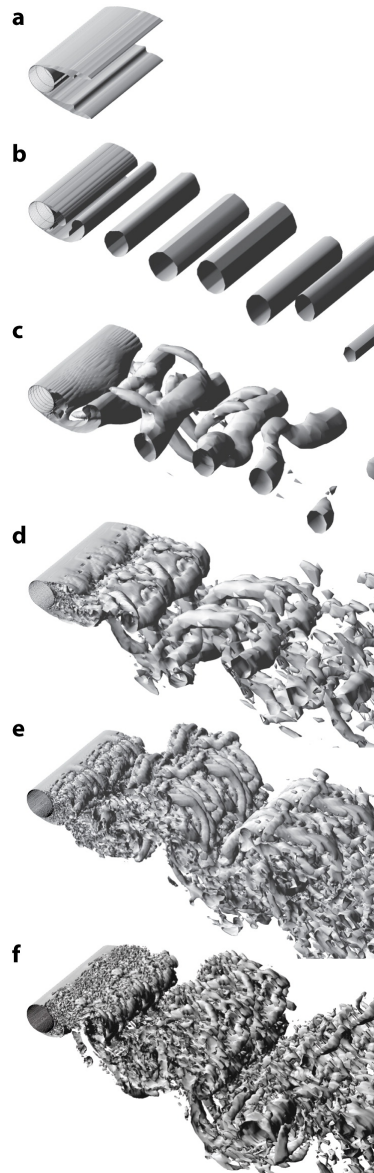


Fig. 15 cylinder les vs rans [13]

grid for LES shown above (actual simulations were DES)



 Spalart PR. 2009.
Annu. Rev. Fluid Mech. 41:181–202

Fig. 16 cylinder simulation with RANS, 2DURANS, 3DURANS, SSTDES, SADES [14]

Vorticity isosurfaces by a circular cylinder: $ReD = 5 \times 10^4$, laminar separation. Experimental drag coefficient $C_d = 1.15\text{--}1.25$. (a) Shear-stress transport (SST) turbulence model steady Reynolds-averaged Navier-Stokes (RANS), $C_d = 0.78$; (b) SST 2D unsteady RANS, $C_d = 1.73$; (c) SST 3D unsteady RANS, $C_d = 1.24$; (d) Spalart-Allmaras (SA) detached-eddy simulation (DES), coarse grid, $C_d = 1.16$; (e) SA DES, fine grid, $C_d = 1.26$; (f) SST DES, fine grid, $C_d = 1.28$. Figure courtesy of A. Travin

illustrates the response of DES to grid refinement in its LES region.

DES solutions with different base RANS models are not sensitive to model choice in the LES region (as opposed to the RANS region, particularly if separation occurs).

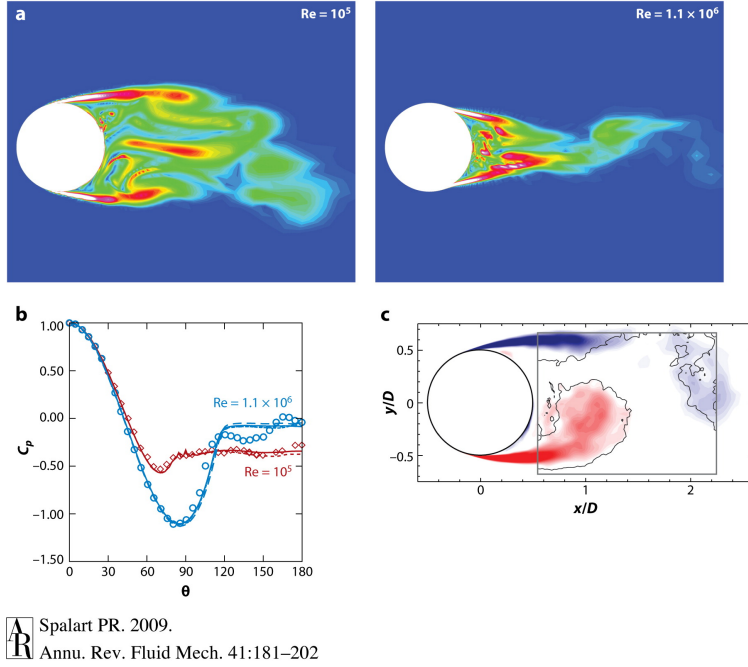


Fig. 17 DES validation from [14]. Sphere transition and drag crisis from [15]. Vorticity validation from [16]

Simple bluff bodies. (a) Flow visualizations and (b) pressure distributions for a sphere. $Re = 105$ and 1.1×106 . Open circles and diamonds denote experiments, whereas the dotted and dashed lines denote detached-eddy simulation (DES) on two grids. Panels a and b courtesy of K. Squires. (c) Phase-averaged vorticity contours for a cylinder. Color gradations denote DES conducted by Mockett et al. (2008), and the solid line denotes experiments by the same authors.

NOTE: DES could be used to emulate the dimples on a golf ball by setting the boundary layer separation point, but true simulation of flow in golf ball dimples requires DNS due to the range of scales

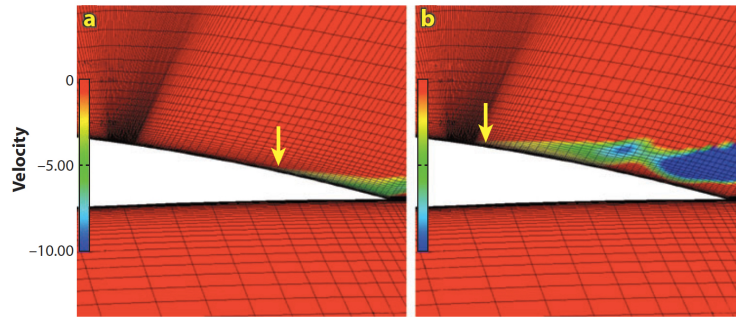


Fig. 18 Example of DES grid induced separation from [14], source: [17]

Vorticity contours over an airfoil: (a) Reynolds-averaged Navier-Stokes and (b) detached-eddy simulation. Arrows indicate separation. Figure taken from Menter & Kuntz 2002.

Potential con of using DES. EXPLAIN HOW GRID INDUCED SEPARATION WORKS.

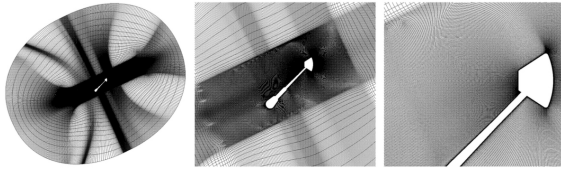


Fig. 19 Orion capsule grid [18]

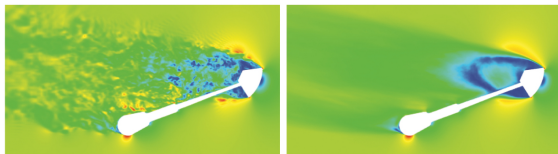


Fig. 20 Orion capsule mach number instantaneous (left) time-averaged (ight) (DES, M=0.5) [18]

Plots of Mach number for an instantaneous and time-averaged solution. For an illustration of the amount of unsteadiness this removed, refer to Fig. 6. It shows a slice of Mach number through the pitch plane ($\phi = 0$ deg) for a DES–KEC solution at Mach 0.50, AoA 170 deg.

RANS did ok compared to WTT/DES for some cases but in others, DES outperformed

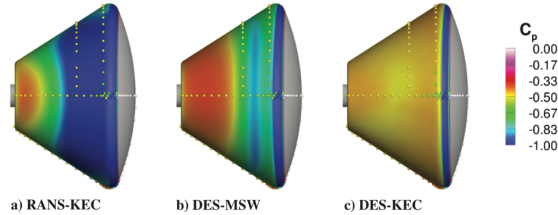


Fig. 21 surface pressure comparison of RANS, DES, WTT, M=0.5 [18]

Freckle plots of pressure tap data, viewed from $\phi = 180$ deg, for Mach 0.50, AoA 155 deg case

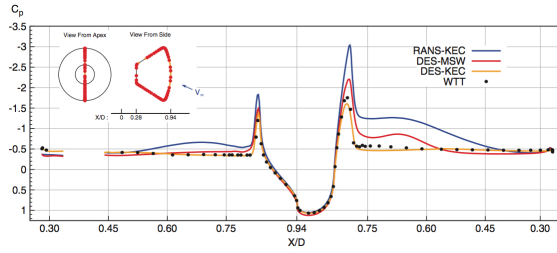


Fig. 22 surface pressure tap comparison of RANS, DES, WTT, M=0.5 [18]

Line plots of pressure tap for data Mach 0.50, AoA 155 deg case.

RANS fails to predict suction peak, surface pressures in wake. Gets best lift integration compared to DES due to separation prediction, worse drag due to wake pressure prediction.

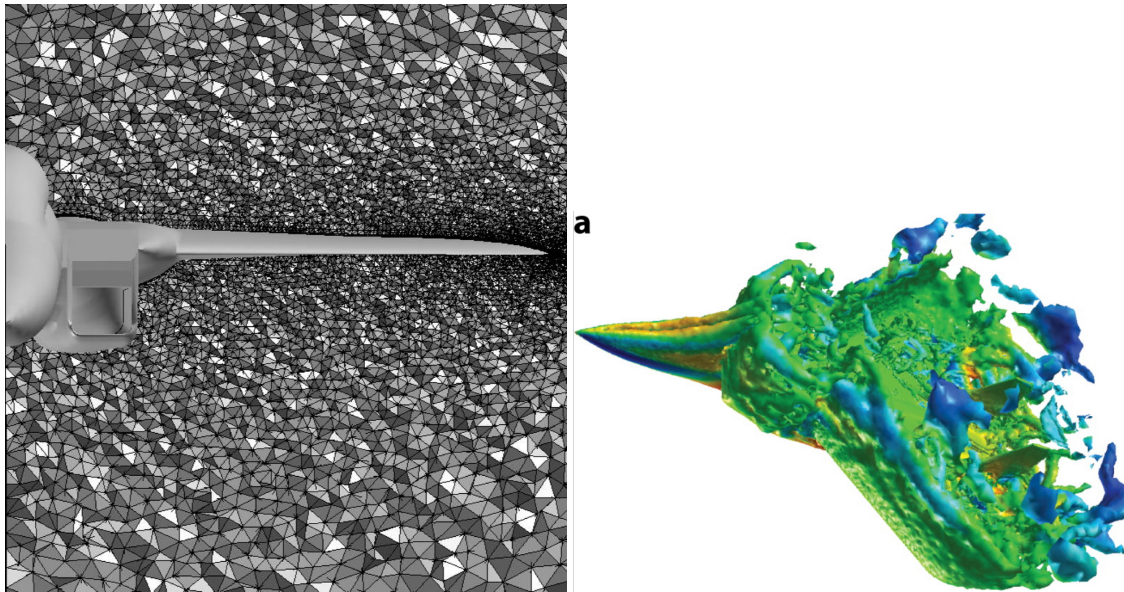


Fig. 23 F-15 DES grid (left) [19] vorticity isocontours (right) [14]

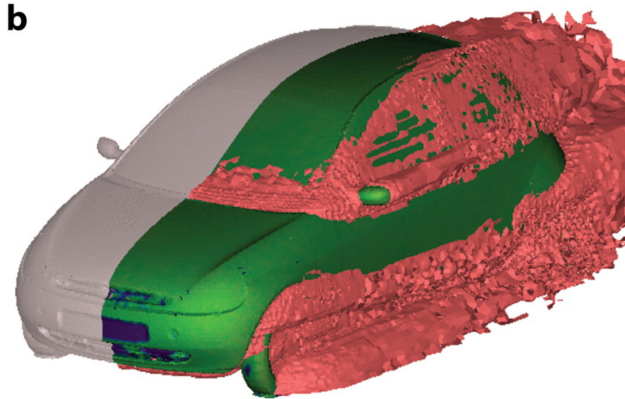


Fig. 24 car DES isocontours [20]

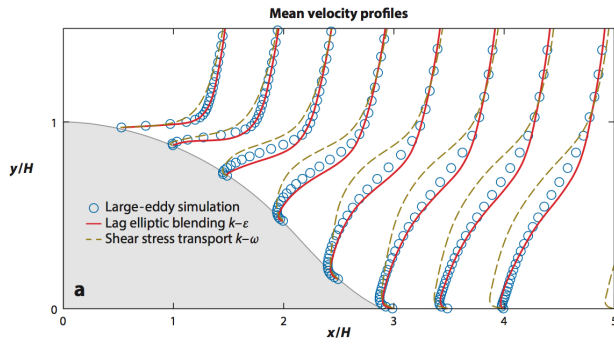


Fig. 25 curve backstep velocity profile les vs rans [21]

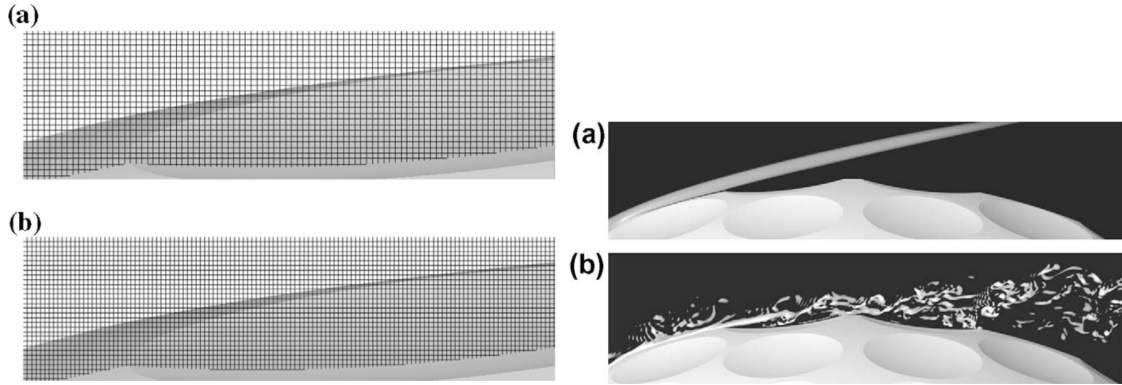


Fig. 26 DNS non-rotating golf ball with dimples grid (left) vorticity (right) [22]

Example grid resolution in a dimple near 84° (measured from the stagnation point at the front of the golf ball). (a) $\text{Re} = 2.5 \cdot 10^4$; (b) $\text{Re} = 1.1 \cdot 10^5$.

Contours of azimuthal vorticity. (a) $\text{Re} = 2.5 \cdot 10^4$; (b) $\text{Re} = 1.1 \cdot 10^5$

NOTE: Recall sphere example from Spalart review and say that this is the analogous DNS experiment to his DES

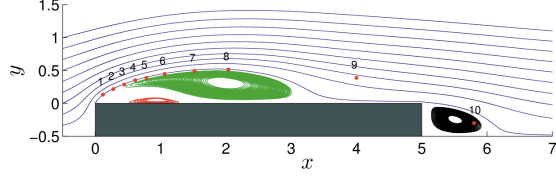


Fig. 27 DNS square cylinder vortex locations Re=3000 [23]

Fig. 4. Streamlines of the mean velocity field (U, V) (x, y) The green lines show the primary vortex, the red lines mark the secondary vortex and the black lines denote the wake vortex. The red dots denote the locations of the probes used for the computation of time spectra in section x5. (For interpretation of the references to color in this figure legend, the reader is referred to the Web version of this article.)

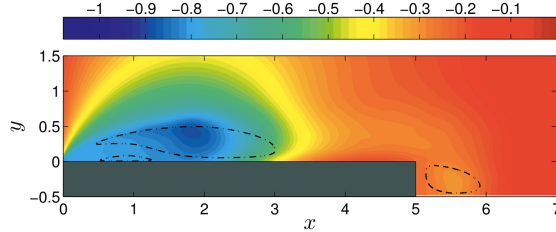


Fig. 28 DNS square cylinder mean pressure distribution Re=3000 [23]

Fig. 5. Isocontours of the mean pressure field $P(x,y)$. The dashed lines report the location of the primary vortex, secondary vortex and wake vortex.

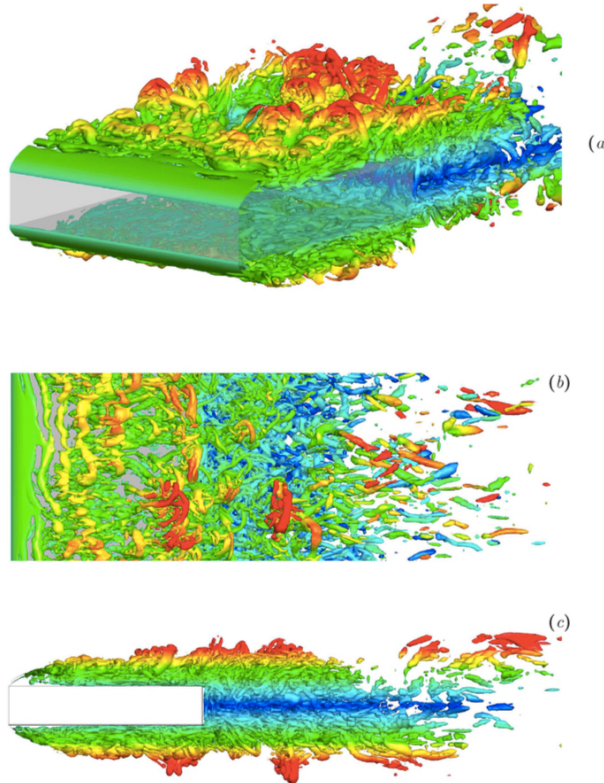


Fig. 29 DNS square cylinder vorticity contours $Re=3000$ [23]

Fig. 10. Instantaneous isosurfaces of $\lambda_2 = -2$ colored with y . Perspective, top and lateral views in (a), (b) and (c) plots, respectively.

VI. Current State of Bluff-Body Turbulence Analysis

- Current State of Knowledge
- Remaining Challenges

A. Experimental Methods

FZ

B. Computational Methods

LH

VII. Conclusions

LH&FZ

Acknowledgments

LH&FZ

Example citations

[24]

References

- [1] Hunt, J., Kawai, H., Ramsey, S., Pedrizetti, G., and Perkins, R., “A review of velocity and pressure fluctuations in turbulent flows around bluff bodies,” *Journal of Wind Engineering and Industrial Aerodynamics*, Vol. 35, 1990, pp. 49 – 85. doi:[https://doi.org/10.1016/0167-6105\(90\)90210-4](https://doi.org/10.1016/0167-6105(90)90210-4), URL <https://www.sciencedirect.com/science/article/pii/0167610590902104>.
- [2] Zdravkovich, M., “Smoke obervations of the formation of a Kármán vortex street,” *Journal of Fluid Mechanics*, Vol. 37, No. 3, 1968, pp. 491 – 496. doi:[doi:10.1017/S0022112069000681](https://doi.org/10.1017/S0022112069000681), URL <https://www.cambridge.org/core/journals/journal-of-fluid-mechanics/article/smoke-observations-of-the-formation-of-a-karman-vortex-street/C9BFB26B8A755EAFFFA6ACC3C91800FB>.
- [3] Gerrard, J. H., “The wakes of cylindrical bluff bodies at low Reynolds number,” *Philosophical transactions of the Royal Society A*, Vol. 288, 1978, pp. 351 – 382. doi:<https://doi.org/10.1098/rsta.1978.0020>, URL <http://rsta.royalsocietypublishing.org/content/288/1354/351.article-info>.
- [4] Zdravkovich, M. M., “Flow around Circular Cylinders; Volume 1. Fundamentals,” *Journal of Fluid Mechanics*, Vol. 350, 1997, p. 375–378. doi:[10.1017/S0022112097227291](https://doi.org/10.1017/S0022112097227291).
- [5] Richardson, L. F., *Weather Prediction by Numerical Process*, Cambridge University Press, Cambridge, UK, 1922.
- [6] Tanaka, S., Takahashi, K., Hosoi, J., and Uchida, M., “Bluff Body Flame Holder with Flow Entrainment Using Perforated Plate,” *9th AIAA/ASME/SAE/ASEE Joint Propulsion Conference*, San Jose, CA, July 2013.
- [7] Li, H., Sung, H., and Yang, V., “Large Eddy Simulation of Combustion Dynamics of Bluff Body Stabilized Flame,” *49th AIAA Aerospace Sciences Meeting including the New Horizons Forum and Aerospace Exposition*, Orlando, Florida, January 2011.
- [8] Ross, J. C., Heineck, J. T., Burnside, N., Sellers, M. E., Halcomb, N., Garbeff, T., Yamauchi, G., and Kushner, L., “Comprehensive Study of the Flow Around a Simplified Orion Capsule Model,” *31st AIAA Applied Aerodynamics Conference*, San Diego, CA, June 2013.
- [9] Yuan, W., Laima, S., Chen, W., Li, H., and Hu, H., “Investigation on the vortex-and-wake-induced vibration of a separated-box bridge girder,” *Journal of Fluids and Structures*, Vol. 70, 2017, pp. 145 – 161. doi:<https://doi.org/10.1016/j.jfluidstructs.2017.01.015>, URL <https://www.sciencedirect.com/science/article/pii/S0889974616304911>.
- [10] Menter, F., and Egorov, Y., “A Scale Adaptive Simulation Model using Two-Equation Models,” *43rd AIAA Aerospace Sciences Meeting and Exhibit, Aerospace Sciences Meetings*, Reno, NV, January 2005.

- [11] Catalano, P., Wang, M., Iaccarino, G., and Moin, P., “Numerical simulation of the flow around a circular cylinder at high Reynolds numbers,” *International Journal of Heat and Fluid Flow*, Vol. 24, No. 4, 2003, pp. 463 – 469. doi:[https://doi.org/10.1016/S0142-727X\(03\)00061-4](https://doi.org/10.1016/S0142-727X(03)00061-4), URL <http://www.sciencedirect.com/science/article/pii/S0142727X03000614>, selected Papers from the Fifth International Conference on Engineering Turbulence Modelling and Measurements.
- [12] Travin, A., Shur, M., Strelets, M., and Spalart, P., “Detached-Eddy Simulations Past a Circular Cylinder,” *Flow, Turbulence and Combustion*, Vol. 63, No. 1, 2000, pp. 293–313. doi:[10.1023/A:1009901401183](https://doi.org/10.1023/A:1009901401183), URL <https://doi.org/10.1023/A:1009901401183>.
- [13] Spalart, P., “Strategies for turbulence modelling and simulations,” *International Journal of Heat and Fluid Flow*, Vol. 21, No. 3, 2000, pp. 252 – 263. doi:[https://doi.org/10.1016/S0142-727X\(00\)00007-2](https://doi.org/10.1016/S0142-727X(00)00007-2), URL <http://www.sciencedirect.com/science/article/pii/S0142727X00000072>.
- [14] Spalart, P. R., “Detached-Eddy Simulation,” *Annual Review of Fluid Mechanics*, Vol. 41, No. 1, 2009, pp. 181–202. doi: [10.1146/annurev.fluid.010908.165130](https://doi.org/10.1146/annurev.fluid.010908.165130), URL <https://doi.org/10.1146/annurev.fluid.010908.165130>.
- [15] Squires, K. D., “Detached-Eddy Simulation: Current Status and Perspectives,” *Direct and Large-Eddy Simulation V*, edited by R. Friedrich, B. J. Geurts, and O. Métais, Springer Netherlands, Dordrecht, 2004, pp. 465–480.
- [16] Mockett, C., Greschner, B., Knacke, T., Perrin, R., Yan, J., and Thiele, F., “Demonstration of Improved DES Methods for Generic and Industrial Applications,” *Advances in Hybrid RANS-LES Modelling*, edited by S.-H. Peng and W. Haase, Springer Berlin Heidelberg, Berlin, Heidelberg, 2008, pp. 222–231.
- [17] Menter, F. R., and Kuntz, M., “Adaptation of Eddy-Viscosity Turbulence Models to Unsteady Separated Flow Behind Vehicles,” *The Aerodynamics of Heavy Vehicles: Trucks, Buses, and Trains*, edited by R. McCallen, F. Browand, and J. Ross, Springer Berlin Heidelberg, Berlin, Heidelberg, 2004, pp. 339–352.
- [18] Schwing, A. M., and Candler, G. V., “Detached-Eddy Simulation of Capsule Wake Flows and Comparison to ind-Tunnel Test Data,” *Journal of Spacecraft and Rockets*, Vol. 52, No. 2, 2015, pp. 439–449.
- [19] Forsythe, J. R., Squires, K. D., Wurtzler, K. E., and Spalart, P. R., “Detached-Eddy Simulation of the F-15E at High Alpha,” *Journal of Aircraft*, Vol. 41, No. 9, 2004, pp. 193–200.
- [20] Mendonça, F., Allen, R., de Charentenay, J., and Lewis, M., “Towards Understanding LES and DES for Industrial Aeroacoustic Predictions,” *International workshop on ‘LES for Acoustics’*, DLR Göttingen, Germany, October 2002.
- [21] Durbin, P. A., “Some Recent Developments in Turbulence Closure Modeling,” *Annual Review of Fluid Mechanics*, Vol. 50, No. 1, 2018, pp. 77–103. doi:[10.1146/annurev-fluid-122316-045020](https://doi.org/10.1146/annurev-fluid-122316-045020).
- [22] Smith, C., Beratlis, N., Balaras, E., Squires, K., and Tsunoda, M., “Numerical investigation of the flow over a golf ball in the subcritical and supercritical regimes,” *International Journal of Heat and Fluid Flow*, Vol. 31, No. 3, 2010, pp. 262 – 273. doi: <https://doi.org/10.1016/j.ijheatfluidflow.2010.01.002>, URL <http://www.sciencedirect.com/science/article/pii/S0142727X10000147>, sixth International Symposium on Turbulence and Shear Flow Phenomena.

- [23] Cimarelli, A., Leonforte, A., and Angeli, D., “Direct numerical simulation of the flow around a rectangular cylinder at a moderately high Reynolds number,” *Journal of Wind Engineering and Industrial Aerodynamics*, Vol. 174, 2018, pp. 39 – 49. doi:<https://doi.org/10.1016/j.jweia.2017.12.020>, URL <http://www.sciencedirect.com/science/article/pii/S0167610517304622>.
- [24] Nakamura, Y., “Bluff-body aerodynamics and turbulence,” *Journal of Wind Engineering and Industrial Aerodynamics*, Vol. 49, No. 1, 1993, pp. 65 – 78. doi:[https://doi.org/10.1016/0167-6105\(93\)90006-A](https://doi.org/10.1016/0167-6105(93)90006-A), URL <http://www.sciencedirect.com/science/article/pii/016761059390006A>.